Rat In A Sphere: Exploring Alternate Grid Cell Representations on a Sphere

Muhammad Sahal Goolam
School of Computer Science and Applied Mathematics
University of the Witwatersrand
Johannesburg, South Africa
Supervised by: Devon Jarvis and Geraud Nangue Tasse

***Abstract*—Grid cells in the medial entorhinal cortex are essential for mammalian spatial navigation, generating regular, hexagonal firing patterns in 2D spaces that function as an internal map. Electrophysiological studies in rats have highlighted that these cells transcend simple spatial layouts, exhibiting sensitivity to environmental geometry and topology as they adapt dynamically to different spatial contexts while preserving their overall regularity. This isotropic behaviour, however, does not extend to 3D space where irregular firing patterns emerge, with the mechanisms underlying spatial cognition beyond planar environments remaining largely unexplored. In this study we explore how spatial encoding strategies may adapt to a curved 2D surface embedded in 3D space and the role of gravity in shaping grid cell patterns. We introduce a novel simulation environment to model a rat's movement in the lower hemisphere of a sphere with adjustable gravitational strengths. Within this framework, we make predictions for different spatial encodings the rat might employ: one aligned with the sphere's curvature and one relative to the horizontal plane beneath the surface, contrasting these under varying gravity. Our findings show that aligning the spatial encoding with the sphere's curvature enhances grid-like behaviour but offers limited localisation ability. In contrast, projecting the environment onto the horizontal plane improves localisation but reduces the regularity of the grid patterns. Additionally, stronger gravitational forces stabilise patterns on the plane and anchor spatial representations toward the base of the sphere, while causing positional shifts when aligned with the sphere's curvature. These results suggest that while aligning grid cells with environmental geometry can support grid-like behaviour, anchoring to gravity in planar contexts may better facilitate natural navigation. Our model establishes a theoretical basis for empirical studies, enabling comparisons with real-world data and extensions to computational models exploring grid cell dynamics[1,2].**

***Index Terms*—Grid cells, Spherical Geometry. Successor Representation**

I. Introduction

Unravelling the neural underpinnings of cognition and spatial navigation remains a core focus in neuroscience. In recent decades, remarkable progress has been made in delineating the neural mechanisms underlying spatial cognition. Research on the mammalian hippocampus and medial entorhinal cortex (MEC), the centres of memory, cognition, and navigation in the brain, has shed light on the brain's remarkable ability to generate intrinsic representations of space [1, 2, 3]. Notably, grid cells [4], specialised neurons in the MEC implicated in spatial encoding, create a strikingly regular, grid-like pattern that effectively tessellates the spatial context an animal occupies. These discoveries have sparked extensive research to characterise these emergent patterns, though a comprehensive understanding of the underlying mechanistic processes remains incomplete.

The behaviour of grid cells has been extensively studied in rats navigating two-dimensional (2D) environments, where they are thought to provide a Euclidean map for spatial navigation [5]. However, recent research suggests that grid cells may encode more than simple spatial maps, responding dynamically to environmental cues, contexts, and topological features, such as food distributions and the geometry of the environment [6, 7]. This evolving understanding has led to a paradigm shift, with grid cells now implicated in encoding predictive spatial representations that integrate these contextual factors [8].

Beyond 2D space, there is growing evidence that grid cells exhibit highly anisotropic behaviour, diverging from the regular, grid-like patterns seen in planar environments [9, 10, 11]. Given that mammals are subject to gravitational forces, it seems natural that such behaviour would arise in non-planar contexts. However, our understanding of how these spatial representations adapt to 3D and non-Euclidean contexts remains vague.

In this work, we begin to address this gap by modelling grid cell behaviour in simulated rats navigating a spherical environment. We contrast different spatial encoding representations a rat might employ on this curved surface and examine the impact of gravitational forces in shaping grid cell behaviour. This is a natural extension from flat surfaces, as we examine an inherently 2D space that operates within a 3D context. To achieve this, we introduce a custom gravity-modulated simulation environment and employ the Successor Representation (SR) model [12], a reinforcement learning framework which has gained attention for its capacity to capture and model the environmental sensitivity of grid cells [8]. Through this, we generate specific predictions about grid cell behaviour on a spherical surface, providing a theoretical foundation for future empirical and simulated research. Our results show distinctive grid cell behaviour under different

[1]This work is currently under review at COSYNE, 2025

[2]We release the code to reproduce the results in this paper at https://github.com/msg3000/RatInASphere

spatial encoding schemes, and implicate gravity as a key factor of anisotropic grid cell emergence in volumetric space. This computational approach opens new avenues for understanding the adaptability of neural representations underlying spatial navigation.

We structure this report as follows: Section II provides foundational background on grid cell behaviour, emphasising empirical findings in both 2D and 3D spaces, along with related work and an overview of the SR model for grid cells. Section III details our experimental setup and simulation environment. In Section IV, we present and interpret the results of the the grid cell predictions, followed by a discussion of their significance and limitations in Section V.

II. Background

A. Entorhinal grid cells

The hippocampus and entorhinal cortex play a central role in the formation of cognitive maps - internal constructs which support memory and navigation [1]. This mapping is realised in the spatial domain through hippocampal place cells [2] and entorhinal grid cells [4]. Place cells have been shown to encode spatial positioning, and respond selectively whenever an animal occupies a particular location in an environment. In contrast, grid cells fire whenever an animal's location coincides with the vertices of a triangular lattice spanning the environmental surface. Grid cells are characterised by their regularly spaced, hexagonal patterns as illustrated in Figure 1.

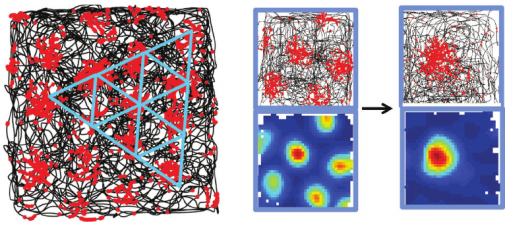

Fig. 1: Empricial grid cell firing in MEC and place cell in hippocampus of a rat navigating a square room [13]. *Left* - Rat's trajectory in the environment shown in black with grid cell spike locations marked in red. *Right* - Grid cell (*left*) and place cell (*right*) activity. *Top* - Trajectory overlaid with spike locations. *Bottom* - Firing rate map, with red indicating high activity and blue indicating low activity.

Extensive research has sought to elucidate the nature of grid cell emergence. Early studies, such as those by Sargolini et al. [5], demonstrated that the MEC integrates information about distance and direction, implicating grid cells in furnishing a global Euclidean representation of space. Recent work, however, has provided evidence that this representation is not purely spatial and cannot account for some of the most striking properties of grid cell firing patterns under certain environmental variations. Stachenfeld et al. [8] propose that the hippocampus encodes a predictive representation of space and is necessarily influenced by both the animal's behaviour and its environmental context. This evolving view implies that grid cell encoding transcends simple spatial layouts, responding dynamically to topological changes.

B. Geometric sensitivity of grid cells

Grid cells in the MEC exhibit a strong sensitivity to the geometry of 2D environments, and empirical evidence has shown that different spatial configurations influence their firing patterns. Studies have shown that in square environments, grid cells form regular, symmetric patterns, while in trapezoidal spaces, these patterns become asymmetrical, revealing a dependence on the specific layout and boundaries of the environment [7]. In circular arenas, grid cell orientations diverge from the axis-aligned patterns seen in squares, further highlighting the influence of well-defined borders [14]. While these findings underscore the responsiveness of grid cells to local geometric cues within a 2D plane [15], they further exhibit the ability to maintain spatial coherence across larger, global structures, even when crossing environmental boundaries [16, 17]. This dual sensitivity to local and global spatial organization suggests that grid cells contribute to a flexible yet unified spatial representation. Expanding upon this, Ulsaker-Janke et al. [18] demonstrated that rodents can develop grid-like firing patterns in spherical environments without prior exposure to prominent landmarks, indicating that rich geometric detail is a catalyst for grid cell expression rather than a basis for it.

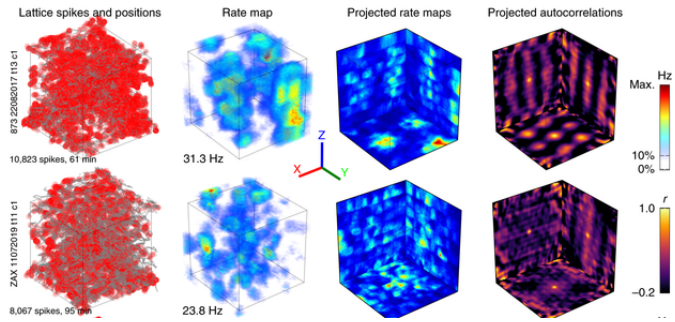

Fig. 2: Experimental results of Grieves et al. [11] of a rat exploring a cubic lattice of two grid cells. (*Left to Right*) Volumetric trajectory of rat (gray) with grid cell spikes (red). Firing rate maps in the environment. Rate maps and spatial autocorrelations projected onto the coordinate planes.These exhibit clear lack of periodicity of firing on the vertical plane, as compared to the horizontal plane.

While the aforementioned findings all underscore the subtlety of grid patterns within planar environments, we remain to discuss its prevalence within 3D space. A reasonable prediction of this would be that grid cells extend their isotropy in 3D forming a hexagonal close packing of spherical fields, however there exists evidence that challenge this prediction. Hayman et al. [9] explores this phenomenon in rats exploring a pegboard and helical environment. While grid patterns were highly regular horizontally, an elongation was observed vertically suggestive that spatial encoding in the brain is anisotropic. Hayman et al. [10] exhibits that in rats foraging within a sloped environment, the resultant grid patterns are similar to those in flat environments with decreased symmetry. This finding suggests a multi-planar representation of space, where grid cells encode spatial information through combining multiple planes at different orientations, rather than a volu-

metric representation that would encompass the continuous 3D space. This hypothesis is expanded by Casali et al. [19] who suggest an interaction between the body plane of the rat (egocentric) and plane of gravity (allocentric) shaping the emergent grid patterns as seen in rats climbing a vertical wall. They observe that more periodic grid cells emerge in the vertical, as contrasted to those exhibited when rats move in the vertical, while remaining horizontally aligned. Furthermore, Grieves et al. [11] examines this within rats exploring a cubic lattice which further displayed irregularity and sparsity in grid patterns while maintaining spatially stable firing patterns, as illustrated in Figure 2. Conjunctively, these works are suggestive of anisotropy in grid patterns that arise with the vertical dimension.

Although experimental studies in rats have shed light on these phenomena, simultaneously recording cellular activity and manipulating environmental geometry presents substantial challenges. As such, several computational models have been proposed that aim to effectively model grid cell activity and derive predictions from it.

C. Successor Representations

Reinforcement Learning (RL) [20] is a framework that models sequential decision making in which an agent interacts with an environment parameterised by a set of states, actions, transition dynamics and reward distributions. The aim of the agent is to learn a policy π, a mapping from states to actions, that maximises the expected cumulative rewards over time. Among several paradigms in RL, the Successor Representation (SR) [12] provides a predictive framework for spatial organisation by encoding future state occupancies through decoupling policy-driven behaviour from environmental rewards. Concretely, for a given state s and policy π, the SR denoted by $M_\pi(s, s')$, represents the discounted sum of future visits to s', starting from s and following π defined as:

$$M_\pi(s, s') = \mathbb{E}\left[\sum_{k=0}^{\infty} \gamma^k \mathbb{1}\{S_{k+t} = s'\} | S_t = s\right], \qquad (1)$$

where γ is the discount factor weighting future state visits and $\mathbb{1}$ is the indicator function and is one when its argument is true and 0 otherwise. In the case of discrete states, the SR is represented as a matrix denoted by M_π.

The work of Stachenfeld et al. [8] highlights a compelling correspondence between the SR and the firing fields of place cells, showing that grid cells encode a spatial map for place cells as a low-dimensional basis derived from the eigenvectors of the SR. Specifically, this is represented by the decomposition: $M_\pi = U\Lambda U^T$ where the columns of U are the eigenvectors of M_π and Λ is a diagonal matrix of their corresponding eigenvalues. This relationship, illustrated in Figure 3, suggests that grid cells form a structured, periodic representation that aligns with the eigenvectors of the SR matrix. Stachenfeld et al. [8] exhibit how the SR is able to parallel a striking number of the characteristics described in Section II-B, however this remains limited to 2D planar environments. We note that the environmental topology and geometric characteristics inherently influence transition dynamics, consequently altering the SR's eigenvectors. This model provides a structured framework to derive and interpret grid cell predictions through the lens of reinforcement learning.

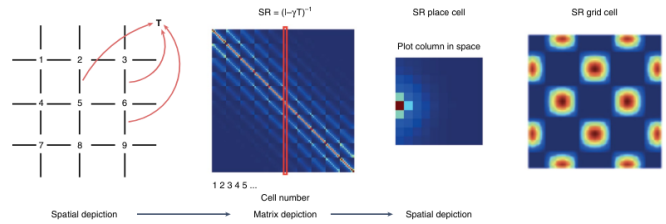

Fig. 3: Grid cells within the successor representation [21]

D. Related work

While the SR has proven effective for modelling grid cell representations in 2D environments, several alternative models have been proposed that display high efficacy in this. In 2D, recurrent neural networks and plasticity-based mechanisms, such as spike-timing dependent plasticity (STDP) [22], have been used to model grid cell activity in networks such as continuous attractor networks [23] and have been shown to approximate the SR in certain contexts [24, 25, 26]. These models, however, generally place explicit assumptions on the latent factors underlying grid cell firing.

In 3D contexts, models specifically address the unique volumetric and anisotropic properties of grid cells. Soman et al. [27] introduce a hierarchical anti-Hebbian network, a type of plasticity model, capturing the anisotropic firing patterns that vary with changes in depth and orientation. Extending this, Gong and Yu [28] proposed a plane-dependent model that is adaptable to both 2D and 3D environments, covering planar, multi-planar, manifold, and volumetric settings. Their model reveals that grid field regularity diminishes as plane perception becomes more uncertain, suggesting a mechanism by which grid cells adapt to complex spatial structures.

Wang et al. [29] further explored grid cell dynamics on smooth 3D manifolds with a gravity-modulated oscillatory model. This approach integrates local (egocentric) and global (allocentric) spatial cues by combining local tangent planes with a gravitational axis, allowing grid patterns to form in alignment with curved, multimodal surfaces. This contrasts with the work of Gong and Yu [28], which assumes that animals perceive motion in a local cylindrical coordinate system projected onto fixed planes aligned with gravity, as opposed to adjusting global coordinates dynamically to align with the surface's curvature.

While these models offer valuable insights into grid cell behaviour in 3D, they rely on explicit representations tied closely to their specific methods—such as plane dependence or oscillatory inputs. In contrast, the SR's implicit encoding of spatial relationships through future state occupancies provides a more flexible and generalised approach, less dependent on

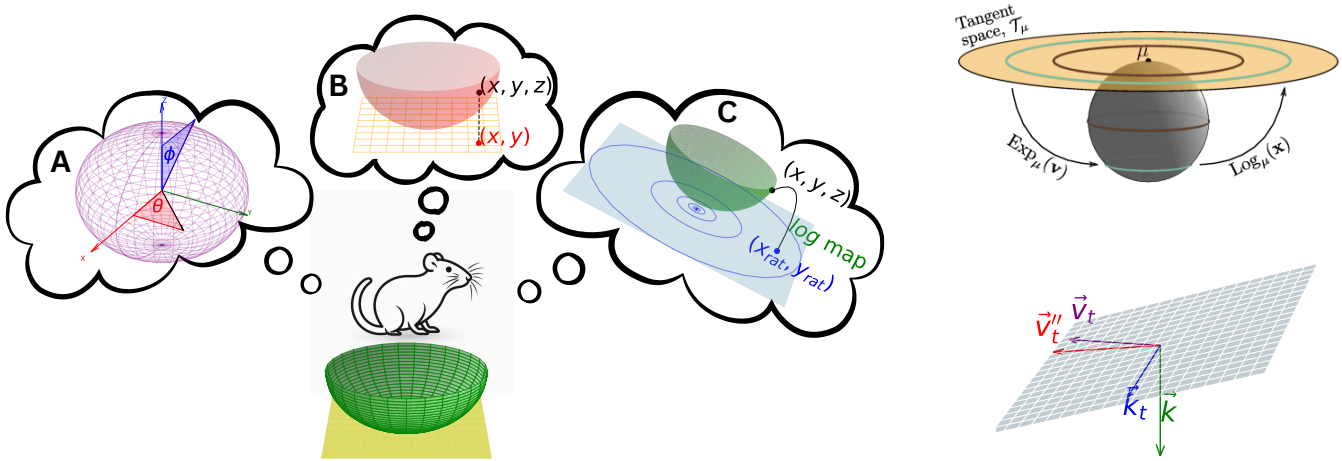

Fig. 4: (*Left*) Potential encodings employed by the rat in a spherical environment. **A** - Spherical coordinates aligning, **B** - Orthogonal projection onto the horizontal plane and **C** - Logarithmic projection onto vertical plane. (*Top Right*) Logarithmic and exponential mappings. The logarithmic map centred at a point maps vectors from the surface of the sphere to the tangent space at that point, and the exponential map performs the inverse mapping of this. The encoding scheme illustrated in **C** applies this logarithmic map centred at the base of the sphere to map the current location to the horizontal plane. (*Bottom Right*) Velocity attenuation conducted in the simulation illustrated on the tangent space at time t. The velocity vector $\boldsymbol{v}_t$ is attenuated in the direction of $\boldsymbol{k}_t$, the projection of the gravity vector $\boldsymbol{k}$ onto the tangent space. This effectively pulls the velocity direction of the rat towards gravity.

explicit structural cues. We thus employ the SR to model grid cell activity extending beyond 2D space.

III. Methods

In this work, we extend the SR model from traditional flat surfaces to a spherical environment. Although embedded in 3D space, this spherical setting remains a 2D manifold, encompassing both horizontal and vertical directions with motion in this space influenced by gravitational pull. Specifically, we simulate a rat navigating the lower hemisphere of this sphere to investigate how spatial representation develops in such a context and its influence on grid cell formation. Through this framework, we explore two key aspects: (1) the nature of spatial representation within this curved manifold and its effect on grid cell patterns, and (2) the role of gravity in shaping these patterns.

A. Encoding regimes

As discussed in Section II-B, proposed spatial encoding schemes have largely been centred in Euclidean representations, with the vertical dimension often excluded. In a spherical environment, however, the shift to non-linear geometry introduces distortions to traditional metrics due to the space's curvature and symmetry. This raises the question of whether spatial encoding is oriented relative to the spherical surface itself or, alternatively, aligns with the gravitational plane below. We contrast three potential encoding strategies to address this: (1) spherical coordinates that track angular deviations in polar and azimuth directions, (2) orthogonal projections of the Euclidean coordinates onto the horizontal plane beneath (see Appendix A), effectively discarding the vertical direction, and (3) a 2D coordinate system using the logarithmic mapping, which operates similar to the orthogonal projection except that it non-linearly expands space with increasing vertical distance. These strategies are illustrated in Figure 4 A,B and C respectively. Notably, we adopt a non-volumetric approach to spatial representation, aligning with the planar framework suggested by Hayman et al. [10], and apply this within a curved setting for further exploration.

B. Simulation environment

To investigate each of these representations, we introduce a simulation environment that enables a rat to traverse the inner surface of a lower hemisphere, under the influence of gravitational pull. This environment is designed using principles of spherical geometry (see Appendix A), enabling egocentric movement of the rat at each timestep while inherently accounting for the curvature of the surface. This contrasts with a similar simulation by Wang et al. [29], in which spatial locations were sampled agnostic to the environment's curvature, with curvature effects instead incorporated into their model of grid cells rather than treated as an environmental characteristic. The detailed dynamics of the simulation are outlined in Algorithm 1.

In this model, the rat's movement is constrained to a spherical surface, ensuring that its path adheres to the curved geometry of the lower hemisphere. At each timestep, the rat randomly selects a velocity direction from the tangent plane to the sphere at its current location. This effectively provides a movement of direction aligned with the body plane of the rat. Gravity, represented by the unit vector $\boldsymbol{k}$, is similarly projected, adding a gravity-aligned component that modifies the rat's velocity. This gravitational component is scaled by g, and can additionally simulate intrinsic surface properties

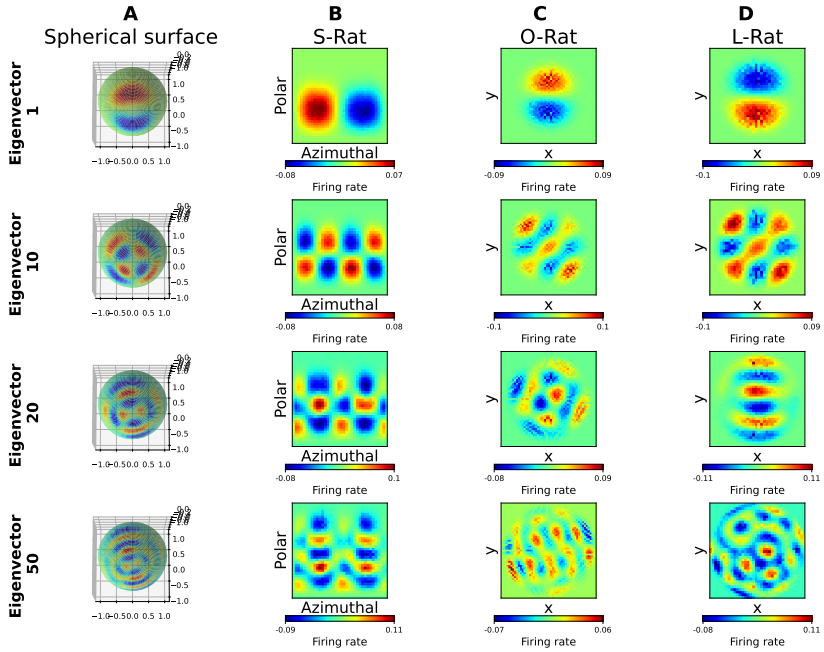

Fig. 5: Grid cell predictions across differing spatial representations for $g = 0.15$. **A** illustrates grid cell firing on the spherical manifold in Euclidean space. This is obtained from the grid cell patterns of S-Rat with the spherical coordinates mapped to 3D space. **B**, **C** and **D** illustrate the grid cell predictions for S-Rat (eigenvectors of SR), O-Rat and L-Rat respectively across various representative grid cells. Note that the polar angles have range $[\pi/2, \pi]$ (top to bottom) from the equator of the hemisphere to the bottom and the azimuthal angles encompass the full revolution. The range of the orthogonal and logarithmic projections are $[-1, 1]$ and $[-1.5, 1.5]$ respectively.

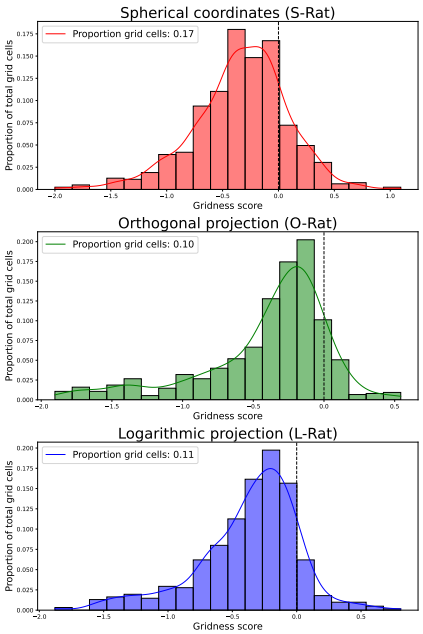

Fig. 6: Histograms of gridness scores across all eigenvectors obtained from S-Rat, O-Rat and L-Rat

Algorithm 1 Rat Simulation on a Lower Hemisphere

Input: Initial position $\boldsymbol{x}_0 \in \mathbb{R}^3$ on the lower hemisphere of unit radius, gravity strength $g \in [0, 1]$, velocity magnitude α
Initialize: Unit vector $\boldsymbol{k} \leftarrow [0, 0, -1]$ pointing in the negative vertical direction (gravity)
for each timestep t **do**
  Randomly select a unit velocity direction $\boldsymbol{v}_t$ from the tangent plane to the sphere at $\boldsymbol{x}_t$
  Project gravity vector $\boldsymbol{k}$ onto the tangent plane to obtain $\boldsymbol{k}_t$
  Compute attenuated velocity: $\boldsymbol{v}_t'' = \boldsymbol{v}_t' + g \cdot \boldsymbol{k}_t$
  Apply exponential map centered at $\boldsymbol{x}_t$ to $\alpha \boldsymbol{v}_t''$
  Update position: $\boldsymbol{x}_{t+1} \leftarrow$ result of exponential map
  if $\boldsymbol{x}_{t+1}$ is in the upper hemisphere **then**
    Invalidate movement and retain $\boldsymbol{x}_t$
  end if
end for

such as friction and drag, or rodent-specific ones such as its mass, adjusting how forcefully gravity influences the rat's path. The velocity is further scaled by α, setting the overall movement velocity. This overall attenuation is illustrated in Figure 4. Starting from the current position, we apply the exponential map to the adjusted velocity, which uses it to move the rat smoothly in the velocity's direction along a geodesic, determining its next location on the spherical surface.

C. Experimental setup

Using this setup, we simulate three rodents randomly navigating the sphere over time, each distinctly employing one of the three spatial representations discussed to highlight differences in their effects. We refer to the rodent tracking the spherical coordinates (ϕ, θ) as S-Rat, the rodent tracking the orthogonal projection (x, y) onto the plane of gravity as O-Rat, and the rodent tracking the logarithmic projection (x', y') of the current location onto the horizontal plane as L-Rat. We additionally simulate a fourth rodent, V-Rat, tracking an orthogonal projection onto the vertical plane parallel with gravity, allowing us to analyse the specific impact of gravitational forces on spatial encoding in the vertical dimension.

Each rodent is simulated over a period time under varying values of g using a standard reinforcement learning framework, in which the agent takes actions and observes state transitions, to estimate each of the SR matrices (see Appendix B for training and implementation details). Each resulting SR matrix is then decomposed into its eigenvectors to obtain the grid cell predictions, which we analyse both qualitatively and quantitatively, as described in the next section.

IV. Results

A. Effect of alternate representations

Our first aim is to examine how alternate spatial representations affect grid cell firing patterns. Figure 5 illustrates grid cell firing patterns on the spherical manifold and grid cell predictions under each of the three representations for fixed

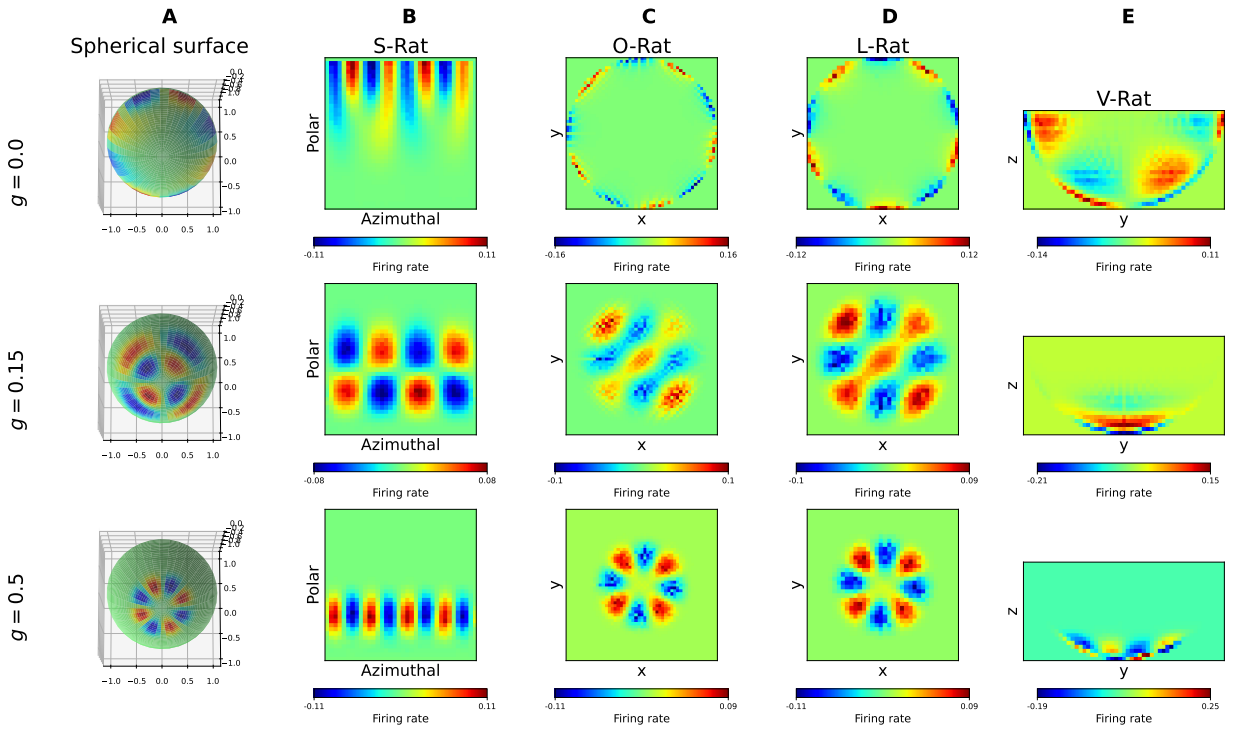

Fig. 7: Grid cell predictions from the SR across different strengths of gravity g for a single eigenvector (eigenvector 10). **A** exhibits grid cell predictions on the spherical surface. **B**, **C** and **D** exhibit elicited grid cell predictions for S-Rat, O-Rat and L-Rat as in Figure 5. **E** depicts grid cell predictions for V-Rat, tracking vertical projections onto the YZ plane with $y \in [-1, 1]$ and $z \in [-1, 0]$.

gravity. We observe varying periodicity in the grid cells within each representation.

As exhibited in Figure 5B, grid cells derived from S-Rat are observed to form generally stable and grid-like firing patterns that align very rigidly to the polar and azimuthal axes. Although the grid cell patterns maintain a regular structure in this coordinate frame, they become highly elongated when mapped onto the spherical surface, as seen in Figure 5A. This distortion stems from the non-linear mapping from spherical to Euclidean coordinates, and is highly pronounced with increases in the vertical dimension. The alignment of the firing patterns with the 2D manifold of the sphere is an expected result, as this parameterisation is isomorphic to a rat navigating a square room, where movement occurs in two basis directions which bound the environment. This suggests that such an encoding scheme inherently supports stable spatial representations by aligning the agent's movement with the underlying geometry.

With respect to the O-Rat and L-Rat encoding schemes, both produce similar grid-like firing patterns but with some differences in spatial distribution as illustrated in Figure 5C,D. The L-Rat exhibits a more expansive pattern, which offers slightly improved stability compared to the orthogonal projection. This primarily arises from L-Rat geometrically unravelling the sphere, while O-Rat merely flattens it. We additionally observe more circular grid cell firing in O-Rat closer towards the centre where the base of the sphere lies, with elongations going outwards. This representation naturally simulates the rat to perceive space as compressed when navigating steeper areas, an effect not observed in the other representations.

In contrast to S-Rat, both O-Rat and L-Rat display varying orientation across different eigenvectors (grid cells).This variation fundamentally arises from the inherent symmetry of the environment when considered in Euclidean space, resulting in grid cells that align in a circular pattern with no strict alignment to any axes. Although less stable, this property reflects findings from the experiment by Stensola et al. [14], where the absence of unique orientation cues in a circular room produced similar effects, highlighting a more ecologically-grounded contrast with the rigid alignment seen in S-Rat.

To further analyse the regularity and structure of grid cell patterns across all representations, we compute the gridness score, a metric that reflects the similarity of firing fields to an ideal hexagonal grid expected of grid cells [8], of all the elicited grid cell predictions. Positive gridness scores indicate stronger grid-like characteristics. Figure 6 shows the distribution of gridness scores for each representation, where S-Rat stands out with a slightly higher average score and a positively skewed distribution, suggesting more pronounced grid-like tendencies. In contrast, O-Rat and L-Rat have similar, but generally lower, gridness score distributions. Notably, S-Rat has the highest proportion of cells with positive grid-

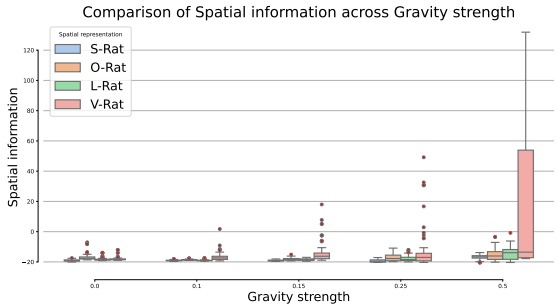

Fig. 8: Boxplots illustrating distribution of spatial information for S-Rat, O-Rat, L-Rat and V-Rat across varying values of gravity.

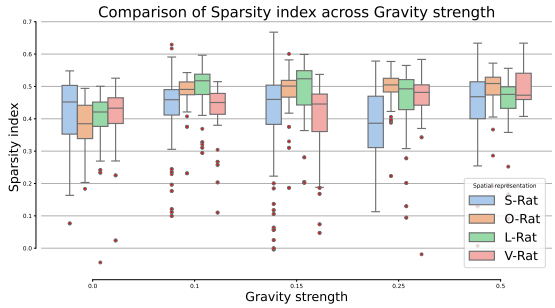

Fig. 9: Boxplots illustrating distribution of sparsity index for S-Rat, O-Rat, L-Rat and V-Rat across varying values of gravity.

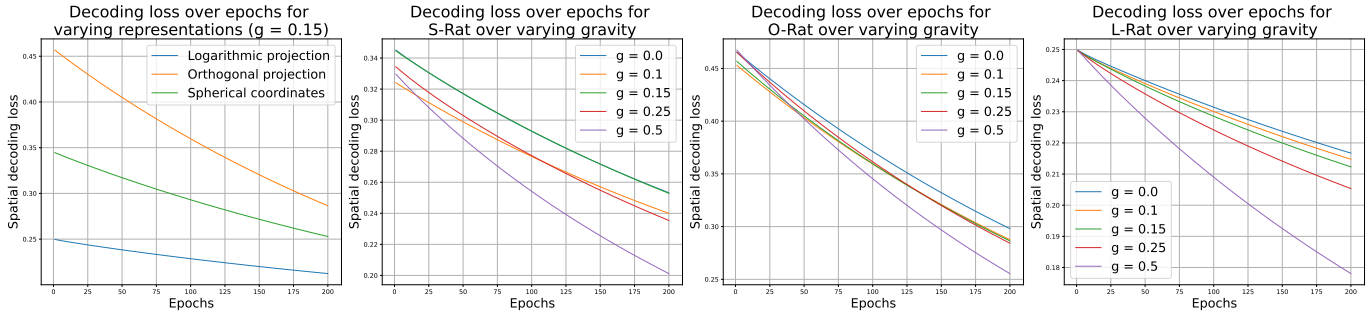

Fig. 10: *Left to Right*: Decoding loss curves of S-Rat, O-Rat and L-Rat for $g = 0.15$ and of each for varying values of gravity

ness scores of 17%, indicating stronger grid-like properties than the other representations, which show only around 10% positive scores. While each representation shows potential for supporting grid-like patterns, these results offers concrete predictions for three alternative encoding strategies that can be experimentally verified.

B. Effect of gravitational forces

We now focus on the effect of varying gravitational strength on grid cell patterns across each representation, illustrated in Figure 7. In Figure 7A we observe the grid patterns on the spherial manifold shift closer towards to the gravitational plane, with less elongation in them as the force of gravity increases. This can be attributed to the lack of activity of the rat in regions higher up due to added difficulty of reaching these points due to gravity, with more structurally apparent grid patterns with the manifold itself converges onto a more planar setting.

In S-Rat, increasing gravity induces a clear translation of grid patterns along the polar axis, with firing patterns remaining relatively stable as exhibited in Figure 7A. This stability again stems from the geometric alignment of this representation to the surface itself, shifting in the direction of gravity. Notably, for $g = 0$, grid cell firing is only partially complete, with patterns resembling those observed in Carpenter et al. [17]'s connected rooms experiment, where spatial constraints led to similar patterns forming. Here, bounding the agent to the lower hemisphere mimics an environmental wall, preventing full grid alignment.

In contrast, this translational effect in S-Rat manifests as a radial contraction of grid cell patterns in O-Rat and L-Rat as gravity increases (Figure 7C and D). This contraction can again be attributed to reduced activity in the upper regions, and the correspondence between the vertical height and radius of the circle at that level. L-Rat again maintains a broader and more pronounced firing field than O-Rat. Interestingly, both models exhibit increasingly circular grid fields under stronger gravitational forces compared to lower gravity levels, where the patterns maintain regularity but tend to be flattened. There is a remarkable bias of the grid fields which point towards the base of the sphere, as seen for $g = 0.5$. Such a tendency suggests a learned environmental adaptation, where grid cells appear to encode a directional bias aligned with gravitational pull, anchoring spatial representations toward the base of the sphere. However we approach such observations with caution.

Although V-Rat is not considered as a representation, we include it here solely to examine the impact of gravitational forces on the vertical plane. In Figure 7E we observe that grid-like behaviour is strongest in the absence of gravity with highly regular structure, but deteriorates significantly as gravitational forces intensify. This suggests that grid cell firing is more isotropic in volumetric space without gravitational influence, strongly indicating the role of downward forces in shaping grid patterns.

C. Localisation

While these results have provided qualitative distinctions between the varying representations and the effect of gravity on them, we remain to examine how these influence the localisation of the rat.

To this end, we computed the spatial information and sparsity index [30, 31] of each grid cell prediction across

the representations and values of gravity to obtain a more holistic overview of there differences. The spatial information is a measure of the amount of information a single grid cell conveys about a location (measured in bits) with a spatial information of 0 indicative of no spatial locality. The sparsity index measures how diffuse the firing is across the spatial domain, ranging from 0 to 1 with 1 being completely uniform firing (see Appendix B).

Figures 8 and 9 illustrate the distributions of these for different representations across varying gravity values. While the individual representations show only marginal differences in both metrics, we observe a consistent increase in spatial information with higher gravity levels. This likely stems from the increased firing increasingly closer to the base of the sphere, effectively localising the rat. Notably, V-Rat demonstrates this effect significantly, with minimal, highly localised firing inducing this. The sparsity index shows high values across all models, with only slight upward trends at stronger gravity levels, yet no consistent patterns emerge. This likely stems from the generally low firing rates observed in each of the grid cell predictions, which do not accurately account for the deviation of the firing at particular location as dependent on how it is computed.

We lastly assessed the sufficiency of each representation (S-Rat, O-Rat, and L-Rat) for accurate localisation to the true (x, y, z) position on the sphere. A simple linear regression model was trained to predict these coordinates based on grid cell firing across all eigenvectors ("grid cells") at each location. This evaluation was conducted for each representation under varying gravity values, with the resulting decoding loss curves shown in Figure 10.

Although qualitative observations suggested similarities between O-Rat and L-Rat, the decoding analysis reveals notable differences. L-Rat achieves the lowest decoding loss with the fastest convergence among the three representations, whereas O-Rat shows the highest decoding loss. This suggests that O-Rat lacks a fully accurate spatial representation, likely due to its disregard for the vertical dimension, which impacts its localisation accuracy. In contrast, L-Rat's geometric configuration enables it to better capture spatial relationships with vertical information embedded in it. S-Rat's performance falls in between, with its higher decoding loss resulting from the mismatch in grid cell encoding in a spherical coordinate frame with decoding in a Euclidean one. The nature of grid cell firing and rigidity of grid alignment potentially causes this, with a misrepresentation of the correct periodicities and orientations limiting the linear decoding.

Regarding gravitational influence, increased gravity values lead to lower decoding loss and improved localisation across all representations, affirming our previous observations. Notably, O-Rat shows more pronounced drops in decoding loss as gravity increases, compared to L-Rat and S-Rat. This can be attributed to higher gravity promoting an increasingly planar region of activity for the rat, making the vertical information that O-Rat discards less crucial under strong gravity.

V. Discussion

Our results reveal four main insights: (1) spatial encoding aligned with underlying geometry (S-Rat) enhances grid-like patterns but offers limited localisation benefits, (2) projecting the environment onto the gravitational plane, particularly with embedded vertical information (L-Rat), improves localisation at a cost to grid regularity, unlike the less effective O-Rat model, (3) stronger gravitational forces enhance grid stability and consistency in the Euclidean representations, anchoring patterns toward the sphere's base, while in the spherical context, they induce only positional shifts, and (4) reduced gravitational influence produces highly regular grid patterns on the vertical plane, suggesting a role in the anisotropic spatial encoding of volumetric space.

While these results provide valuable insights, several limitations warrant discussion. First, there is no empirical evidence that rat grid cells operate within a spherical or non-Euclidean coordinate frame. Although our findings reflect a planar analogy to a square room, a biological mechanism for such coordinate remapping is unproven. Furthermore, the rigid alignment of grid cells to the azimuth seems inconsistent, given the environment's symmetry. While alignment with the polar axis might be expected due to gravitational orientation, azimuthal alignment lacks a clear rationale. While the logarithmic projection enhances localisation by integrating vertical information, the orthogonal model disregards it, despite vertical cues being essential. However, this perfect geometric mapping remains unfounded. This may manifest in rats as a multi-planar representation, as suggested by Hayman et al. [10], where the orthogonal projection serves as a ground reference and the varying alignment of the body plane of the rat to the axis of gravity influences grid cell firing. Shinder and Taube [32] evidence a very similar encoding basis with regards to head-direction tuning. Alternatively, this could be shaped by visual inputs which would support the variable grid cell orientation due to the uniformity of the environment.

We are further limited by our simulation environment which necessarily includes several simplifications. The assumption of random motion reduces computational demands, but diverges from the goal-directed navigation typical of rats [33] that integrates path information and directional heading observed in rats [34]. Additionally, rats have in several studies exhibited a preference to not engage in vertical motion [9, 35], suggesting that they would remain within a very close vicinity of the spherical base, traversing upwards only for food-driven purposes. A second limitation of our simulation is the simplistic gravity attenuation, which lacks an accounting for more complex physical dynamics and an application of this within a correct scale. This, however, has the merit of abstracting complex detail and can easily be interpreted as a modulation of the slipperiness of a surface or the weight of rats. While gravity cannot effectively be easily modulated, these properties form concrete case studies from which our model can generate predictions.

We are additionally constrained by the ambiguous nature of

spatial encoding in 3D, particularly concerning the processing of vertical spatial information. This challenge is compounded by a limited number of empirical studies. While Ulsaker-Janke et al. [18] recorded data in rats exploring a spherical environment, their exploration was planar, without vertical interaction, making comparisons with real neural data difficult. Additionally, while gridness score serves to provide a quantitative measure of grid-like behaviour, it is not a very robust metric with several qualitatively grid-like patterns (see Figure 12) scoring very poorly.

While the SR model shows promise for simulating grid cell behaviour, it has inherent limitations, particularly its instability under changing policies and goals. The Linear RL model proposed by Piray and Daw [36] addresses this by introducing greater robustness to behavioural shifts, aligning more closely with grid cells' adaptive nature. Although SR learning methods are traditionally analytic or iterative, newer deep learning approaches face challenges due to limited empirical support from hippocampal networks [26]. Continuous attractor network models may offer a more biologically consistent alternative by naturally capturing the spatial continuity characteristic of grid cell activity.

This work opens multiple pathways for further investigation. First, refining the simulation to incorporate more realistic dynamics, such as a physics engine for gravitational effects and friction, could enhance the ecological validity of our findings and better approximate real-world navigation challenges. Extending the environment beyond spherical geometry—exploring hyperbolic or other curved surfaces—could also provide valuable insights into the adaptability of grid cells under different spatial constraints. Moreover, recent developments in virtual reality (VR) indicate that environmental cues significantly influence grid cell alignment [37]. Leveraging VR-based experiments could enable controlled studies on the influence of local movements and visual cues, potentially verifying the model's predictions in dynamic, immersive contexts. Finally, validating these computational predictions with empirical studies, as discussed, would be incredibly valuable. By grounding the models in experimental data, future research can clarify the capacity of existing models to accurately capture grid cell behaviour.

In conclusion, this study introduces a model for understanding grid cell behaviour in a spherical environment, offering key insights into how spatial encoding might adapt to curved surfaces and gravitational forces. By investigating multiple representations and gravitational conditions, our findings contribute to a more comprehensive view of spatial cognition beyond traditional planar settings. We hope that these insights set the stage for future research into adaptive spatial encoding and deepen our understanding of the neural mechanisms that underpin spatial navigation in diverse environmental contexts.

References

[1] E. C. Tolman, "Cognitive maps in rats and men." *Psychological review*, vol. 55, no. 4, p. 189, 1948.

[2] J. O'Keefe and J. Dostrovsky, "The hippocampus as a spatial map: preliminary evidence from unit activity in the freely-moving rat." *Brain research*, 1971.

[3] J. S. Taube, R. U. Muller, and J. B. Ranck, "Head-direction cells recorded from the postsubiculum in freely moving rats. i. description and quantitative analysis," *Journal of Neuroscience*, vol. 10, no. 2, pp. 420–435, 1990.

[4] T. Hafting, M. Fyhn, S. Molden, M.-B. Moser, and E. I. Moser, "Microstructure of a spatial map in the entorhinal cortex," *Nature*, vol. 436, no. 7052, pp. 801–806, 2005.

[5] F. Sargolini, M. Fyhn, T. Hafting, B. L. McNaughton, M. P. Witter, M.-B. Moser, and E. I. Moser, "Conjunctive representation of position, direction, and velocity in entorhinal cortex," *Science*, vol. 312, no. 5774, pp. 758–762, 2006.

[6] R. U. Muller and J. L. Kubie, "The effects of changes in the environment on the spatial firing of hippocampal complex-spike cells," *Journal of Neuroscience*, vol. 7, no. 7, pp. 1951–1968, 1987.

[7] J. Krupic, M. Bauza, S. Burton, C. Barry, and J. O'Keefe, "Grid cell symmetry is shaped by environmental geometry," *Nature*, vol. 518, no. 7538, pp. 232–235, 2015.

[8] K. L. Stachenfeld, M. M. Botvinick, and S. J. Gershman, "The hippocampus as a predictive map," *Nature neuroscience*, vol. 20, no. 11, pp. 1643–1653, 2017.

[9] R. Hayman, M. A. Verriotis, A. Jovalekic, A. A. Fenton, and K. J. Jeffery, "Anisotropic encoding of three-dimensional space by place cells and grid cells," *Nature neuroscience*, vol. 14, no. 9, pp. 1182–1188, 2011.

[10] R. M. Hayman, G. Casali, J. J. Wilson, and K. J. Jeffery, "Grid cells on steeply sloping terrain: evidence for planar rather than volumetric encoding," *Frontiers in psychology*, vol. 6, p. 925, 2015.

[11] R. M. Grieves, S. Jedidi-Ayoub, K. Mishchanchuk, A. Liu, S. Renaudineau, É. Duvelle, and K. J. Jeffery, "Irregular distribution of grid cell firing fields in rats exploring a 3d volumetric space," *Nature neuroscience*, vol. 24, no. 11, pp. 1567–1573, 2021.

[12] P. Dayan, "Improving generalization for temporal difference learning: The successor representation," *Neural computation*, vol. 5, no. 4, pp. 613–624, 1993.

[13] M.-B. Moser, D. C. Rowland, and E. I. Moser, "Place cells, grid cells, and memory," *Cold Spring Harbor perspectives in biology*, vol. 7, no. 2, p. a021808, 2015.

[14] T. Stensola, H. Stensola, M.-B. Moser, and E. I. Moser, "Shearing-induced asymmetry in entorhinal grid cells," *Nature*, vol. 518, no. 7538, pp. 207–212, 2015.

[15] J. Krupic, M. Bauza, S. Burton, and J. O'Keefe, "Local transformations of the hippocampal cognitive map," *Science*, vol. 359, no. 6380, pp. 1143–1146, 2018.

[16] D. Derdikman, J. R. Whitlock, A. Tsao, M. Fyhn, T. Hafting, M.-B. Moser, and E. I. Moser, "Fragmentation of grid cell maps in a multicompartment environment," *Nature neuroscience*, vol. 12, no. 10, pp. 1325–1332, 2009.

[17] F. Carpenter, D. Manson, K. Jeffery, N. Burgess, and C. Barry, "Grid cells form a global representation of connected environments," *Current Biology*, vol. 25, no. 9, pp. 1176–1182, 2015.

[18] I. Ulsaker-Janke, T. Waaga, T. Waaga, E. I. Moser, and M.-B. Moser, "Grid cells in rats deprived of geometric experience during development," *Proceedings of the National Academy of Sciences*, vol. 120, no. 41, p. e2310820120, 2023.

[19] G. Casali, D. Bush, and K. Jeffery, "Altered neural odometry in the vertical dimension," *Proceedings of the national academy of sciences*, vol. 116, no. 10, pp. 4631–4636, 2019.

[20] R. S. Sutton and A. G. Barto, *Reinforcement learning: An introduction*. MIT press, 2018.

[21] J. C. Whittington, D. McCaffary, J. J. Bakermans, and T. E. Behrens, "How to build a cognitive map," *Nature neuroscience*, vol. 25, no. 10, pp. 1257–1272, 2022.

[22] H. Markram, W. Gerstner, and P. J. Sjöström, "Spike-timing-dependent plasticity: a comprehensive overview," *Frontiers in synaptic neuroscience*, vol. 4, p. 2, 2012.

[23] O. Shipston-Sharman, L. Solanka, and M. F. Nolan, "Continuous attractor network models of grid cell firing based on excitatory–inhibitory interactions," *The Journal of physiology*, vol. 594, no. 22, pp. 6547–6557, 2016.

[24] A. C. Schapiro, N. B. Turk-Browne, M. M. Botvinick, and K. A. Norman, "Complementary learning systems within the hippocampus: a neural network modelling approach to reconciling episodic memory with statistical learning," *Philosophical Transactions of the Royal Society B: Biological Sciences*, vol. 372, no. 1711, p. 20160049, 2017.

[25] C. Fang, D. Aronov, L. Abbott, and E. L. Mackevicius, "Neural learning rules for generating flexible predictions and computing the successor representation," *Elife*, vol. 12, p. e80680, 2023.

[26] T. M. George, W. de Cothi, K. L. Stachenfeld, and C. Barry, "Rapid learning of predictive maps with stdp and theta phase precession," *Elife*, vol. 12, p. e80663, 2023.

[27] K. Soman, S. Chakravarthy, and M. M. Yartsev, "A hierarchical anti-hebbian network model for the formation of spatial cells in three-dimensional space," *Nature communications*, vol. 9, no. 1, pp. 1–15, 2018.

[28] Z. Gong and F. Yu, "A plane-dependent model of 3d grid cells for representing both 2d and 3d spaces under various navigation modes," *Frontiers in Computational Neuroscience*, vol. 15, p. 739515, 2021.

[29] Y. Wang, X. Xu, X. Pan, and R. Wang, "Grid cell activity and path integration on 2-d manifolds in 3-d space," *Nonlinear Dynamics*, vol. 104, pp. 1767–1780, 2021.

[30] W. Skaggs, B. Mcnaughton, and K. Gothard, "An information-theoretic approach to deciphering the hippocampal code," *Advances in neural information processing systems*, vol. 5, 1992.

[31] M. W. Jung, S. I. Wiener, and B. L. McNaughton, "Comparison of spatial firing characteristics of units in dorsal and ventral hippocampus of the rat," *Journal of Neuroscience*, vol. 14, no. 12, pp. 7347–7356, 1994.

[32] M. E. Shinder and J. S. Taube, "Three-dimensional tuning of head direction cells in rats," *Journal of neurophysiology*, vol. 121, no. 1, pp. 4–37, 2019.

[33] M. Sosa and L. M. Giocomo, "Navigating for reward," *Nature Reviews Neuroscience*, vol. 22, no. 8, pp. 472–487, 2021.

[34] T. L. Bjerknes, N. C. Dagslott, E. I. Moser, and M.-B. Moser, "Path integration in place cells of developing rats," *Proceedings of the National Academy of Sciences*, vol. 115, no. 7, pp. E1637–E1646, 2018.

[35] H. Schiffman, R. Lore, J. Passafiume, and R. Neeb, "Role of vibrissae for depth perception in the rat (rattus norvegicus)," *Animal behaviour*, vol. 18, pp. 290–292, 1970.

[36] P. Piray and N. D. Daw, "Linear reinforcement learning in planning, grid fields, and cognitive control," *Nature communications*, vol. 12, no. 1, p. 4942, 2021.

[37] X. Yang, F. Cacucci, N. Burgess, T. J. Wills, and G. Chen, "Visual boundary cues suffice to anchor place and grid cells in virtual reality," *Current Biology*, vol. 34, no. 10, pp. 2256–2264, 2024.

[38] C. C. Domine, R. A. Carrasco Davis, L. Hollingsworth, N. Sirmpilatze, A. L. Tyson, D. Jarvis, C. Barry, and A. M. Saxe, "Neuralplayground: A standardised environment for evaluating models of hippocampus and entorhinal cortex," *bioRxiv*, pp. 2024–03, 2024.

APPENDIX

We structure the supplementary material as follows: Appendix A details mathematical background in Euclidean and Spherical Geometry. Appendix B presents technical details for reproducibility regarding the simulation, as well as on the calculation of the evaluation metrics. Appendix C shows extended and supplementary figures of the results presented.

APPENDIX A
RIEMANNIAN GEOMETRY

A. Spherical Geometry

The unit sphere $\mathbb{S}^2$ is defined by:

$$\mathbb{S}^2 = \{\boldsymbol{x} \in \mathbb{R}^3 | \|\boldsymbol{x}\| = 1\}, \tag{2}$$

and is parameterised by (ϕ, θ), where $\phi \in [0, \pi]$ is the polar angle and $\theta \in [0, 2\pi)$ is the azimuthal angle, so that the Euclidean coordinates of each point $\boldsymbol{x} \in \mathbb{S}^2$ is given by:

$$\boldsymbol{x}(\phi, \theta) = [sin(\phi)cos(\theta), sin(\phi)sin(\theta), cos(\phi)]^T. \tag{3}$$

As such, $\mathbb{S}^2$ is a 2D manifold embedded in 3D space. Within this work we restrict ourselves to the lower hemisphere which we denote as $\mathbb{S}^2_-$ such that $\phi \in [\frac{\pi}{2}, \pi]$.

For a real, smooth manifold M, the tangent space at a point $\boldsymbol{p} \in M$ denoted by $\mathcal{T}_{\boldsymbol{p}}M$ is a vector space defined as a flat plane that consists the set of tangent vectors to M at $\boldsymbol{p}$. Within the context of this research, the manifold is the sphere $\mathbb{S}^2$. A point $\boldsymbol{q}$ on the sphere (the rats location) can be mapped to the tangent space at point $\boldsymbol{p}$, $\mathcal{T}_{\boldsymbol{p}}\mathbb{S}^2$, via the logarithmic map $log_{\boldsymbol{p}} : \mathbb{S}^2 \to \mathcal{T}_{\boldsymbol{p}}\mathbb{S}^2$ given by:

$$log_{\boldsymbol{p}}(\boldsymbol{q}) = (\boldsymbol{q} - \boldsymbol{p}(\boldsymbol{q}^T\boldsymbol{p}))\frac{\theta}{sin(\theta)}, \tag{4}$$

where $\theta = arccos(\boldsymbol{q}^T\boldsymbol{p})$. The inverse mapping which maps a tangent vector $\boldsymbol{v}$ back to the sphere is given by the exponential map $exp_{\boldsymbol{p}} : \mathcal{T}_{\boldsymbol{p}}\mathbb{S}^2 \to \mathbb{S}^2$ and can be derived as:

$$exp_{\boldsymbol{p}}(\boldsymbol{v}) = cos(\|\boldsymbol{v}\|)\boldsymbol{p} + sin(\|\boldsymbol{v}\|)\frac{\boldsymbol{v}}{\|\boldsymbol{v}\|}. \tag{5}$$

Both maps provide a mechanism of mapping points between the tangent space and the spherical surface. For the purposes of tracking spatial information, we employ the logarithmic map to map the current location of the rat on the sphere, to the instantaneous tangent space that determines its next movement. Within the context of the simulation, we employ the exponential map at the current location to map the velocity vector in the tangent space to obtain the updated location. The logarithmic map is also indirectly utilised to map the pre-transition location to the tangent space. We note that the application of the logarithmic map $log_{\boldsymbol{p}}$ to the point $\boldsymbol{p}$ yields

$$log_{\boldsymbol{p}}(\boldsymbol{p}) = (\boldsymbol{p} - \boldsymbol{p}(\boldsymbol{p}^T\boldsymbol{p}))\frac{\theta}{sin(\theta)} = (\boldsymbol{p} - \boldsymbol{p})\frac{\theta}{sin(\theta)} = \boldsymbol{0},$$

since $\boldsymbol{p}^T\boldsymbol{p} = \|\boldsymbol{p}\| = 1$ and the singularity at $\theta = arccos(1) = 0$ is treated with the convention $\frac{0}{sin(0)} = 1$. As such, a step of size α along a vector $\boldsymbol{v}$ in the tangent plane yields $\alpha\boldsymbol{v}$.

B. Orthogonal projection in Euclidean space

In the Euclidean space $\mathbb{R}^3$, the orthogonal projection of a vector $\boldsymbol{x} \in \mathbb{R}^3$ onto a plane with unit normal $\boldsymbol{n}$ is given by:

$$orth_{\boldsymbol{n}}\boldsymbol{x} = \boldsymbol{x} - (\boldsymbol{x}^T\boldsymbol{n})\boldsymbol{n}. \tag{6}$$

In the case that the unit normal to the tangent plane is $\boldsymbol{k} = (0, 0, -1)^T$, the orthogonal projection onto a vector $\boldsymbol{x}$ defines a mapping $(x, y, z) \to (x, y, 0)$, effectively discarding the vertical dimension.

C. Orthogonal vs Logarithmic projection

The orthogonal and logarithmic projections utilised in this work operate identically, with the except of a non-linear scaling in the logarithmic mapping. For the rat occupying location $\boldsymbol{x}_t = (x, y, z)$ on the unit sphere, the normal to the tangent plane to the sphere at $\boldsymbol{x}_t$ is given by $\boldsymbol{x}_t$ and hence the logarithmic projection onto the horizontal plane at the base of the sphere $\boldsymbol{k} = (0, 0, -1)^T$ is given by:

$$\begin{aligned} log_{\boldsymbol{k}}(\boldsymbol{x}_t) &= (\boldsymbol{x}_t - \boldsymbol{k}(\boldsymbol{x}_t^T\boldsymbol{k}))\frac{\theta}{sin(\theta)} \\ &= (\boldsymbol{x}_t - z\boldsymbol{k})\frac{\theta}{sin(\theta)} \\ &= \frac{\theta}{sin(\theta)}(x, y, 0)^T, \end{aligned} \tag{7}$$

which is identical to the orthogonal projection onto the horizontal plane, with the exception of the scaling factor $\frac{\theta}{sin(\theta)}$ where $\theta = arccos(\boldsymbol{x}_t^T\boldsymbol{k}) = arccos(-z)$. For $z \in [-1, 0]$, we have $\theta \in [0, \frac{\pi}{2}]$ increasing vertical height from the base of the sphere. The function $\frac{\theta}{sin(\theta)}$ then increases non-linearly over this interval, scaling the orthogonal projection higher as the vertical elevation increases.

APPENDIX B
TECHNICAL AND EXPERIMENTAL DETAILS

A. Problem setup

Problems in reinforcement learning are modelled as a Markov Decision Process (MDP) [20]. An MDP is defined as a 4-tuple, $\langle \mathcal{S}, \mathcal{A}, \mathcal{T}, \mathcal{R} \rangle$, where $\mathcal{S}$ is the set of states, $\mathcal{A}$ is the the set of actions, $\mathcal{T} : \mathcal{S} \times \mathcal{A} \times \mathcal{S} \to [0, 1]$ is the transition function, where $P(s'|s, a)$ represents the probability of being in state s' after taking action a in state s, and $\mathcal{R} : \mathcal{S} \to \mathbb{R}$ is the reward function.

State space representation

For the purposes of this research, we discretise the continuous space $\mathbb{S}^2_-$ and reparameterise the environment in terms of spherical coordinates. The polar and azimuth angles, ϕ and θ, are discretised into N_ϕ and N_θ equal, evenly spaced points respectively. The resultant state space, $\mathcal{S}$ then has $|\mathcal{S}| = N_\phi \times N_\theta$.

Actions
The action space of the rat is the set $[0,1]^3$, from which the rat uniformly selects a velocity vector at each timestep, i.e. the velocity vector $\boldsymbol{v} = [v_x, v_y, v_z]$ is sampled according from a $U(0,1)$ distribution. This allows for uniform random motion over the sphere.

Transition dynamics
A necessary condition for the rat remaining constrained to the surface of the sphere is that the velocity direction lies on the instantaneous tangent plane to the sphere at the current location $\boldsymbol{x}_t$. To ensure this, we orthogonally project the velocity vector onto the tangent plane whose unit normal is also given by $\boldsymbol{x}_t$ through:

$$proj_{\boldsymbol{x}_t}\boldsymbol{v}_t = \boldsymbol{v}_t - (\boldsymbol{v}_t^T\boldsymbol{x}_t)\boldsymbol{x}_t, \tag{8}$$

which combined with the action selection samples a vector from the current tangent plane. This vector is then normalised and a similar projection is done to the unit vector $\boldsymbol{k} = [0,0,-1]$ to obtain the gravity vector that accounts for the alignment between the plane and the direction of gravity. The attenuated velocity and exponential map are then computed as described in Algorithm 1. The next state $\boldsymbol{x}_{t+1}$ is then converted into spherical coordinates and clamped to the nearest value to match the discretisation described above.

SR Matrix and Learning
The SR matrix , M, is learnt using tabular methods such that $M \in \mathbb{R}^{|S|\times|S|}$. As the rat traverses the environment, we update the SR matrix through:

$$\begin{aligned} M(s_t, s') \leftarrow M(s_t, s') + \eta(\mathbb{1}\{s_t = s'\} \\ + \gamma M(s_{t+1}, s') - M(s_t, s')), \end{aligned} \tag{9}$$

where $s_t \rightarrow s_{t+1}$ is the observed transition, η is the learning rate, γ is the discount factor and s' denotes all other states.

B. Hyperparameters

For the environment in which S-Rat is simulated, we utilise a smaller discretisation, compared to that of O-Rat and L-Rat. This is done due to the difference in the SR representations of each. The spherical agent has an explicit dependence on this discretisation with the state space growing linearly with their product and the SR quadratically. In contrast, the other representations do not have such a dependence, but rather discretise the horizontal plane beneath. These hyperparameters, as well as training hyperparameters are summarised in Table I.

C. Metrics

1) Gridness score calculation: The periodicity of the grid patterns is quantified using the gridness score [5] given by:

$$\begin{aligned} \text{Gridness score} = min\{\ cor(\boldsymbol{r}, \boldsymbol{r}_{60}), cor(\boldsymbol{r}, \boldsymbol{r}_{120})\} \\ - max\{\ cor(\boldsymbol{r}, \boldsymbol{r}_{30}), cor(\boldsymbol{r}, \boldsymbol{r}_{90}), cor(\boldsymbol{r}, \boldsymbol{r}_{150})\}, \end{aligned} \tag{10}$$

TABLE I: Simulation hyperparameters of each representation for reproducibility

Hyperparameter	Value
Training steps	10^6
Learning rate η	0.01
Discount factor γ	0.9
Agent seed (random policy)	42
N_ϕ, N_θ (S-Rat only)	36
N_ϕ, N_θ (O-Rat, L-Rat and V-Rat)	100
Grid cell resolution (all)	36×36

where cor is Pearson's correlation and r_θ is the rotated autocorrelation map by $\theta°$. This effectively aims to measure the observed difference between grid patterns and that of a hexagonal grid field.

2) Spatial information and sparsity index calculation: The spatial information and sparsity index is calculated as follows:

$$\text{Spatial Info.} = \sum_i p_i \cdot \frac{\lambda_i}{\lambda} \cdot log_2(\frac{\lambda_i}{\lambda}) \tag{11}$$

$$\text{Sparsity Index} = \frac{(\sum_i p_i\lambda_i)^2}{(\sum_i p_i\lambda_i^2)}, \tag{12}$$

where i ranges over the discretised bins the rat occupies, p_i is the probability the rat is in bin i (estimated using frequency count), λ_i is the firing rate in bin i and λ is the mean firing rate across the space.

D. Grid cell decoding experiment

In our grid cell decoding experiment, we train a simple linear regression utilising the eigenvectors of each representation. Each location in the grid cell map is mapped onto its Euclidean coordinates in 3D space. For S-Rat this is done using Equation 3, for O-Rat as well we utilise this to recover the z-coordinate and for L-Rat using the exponential map. The training hyperparameters are depicted in Table II.

TABLE II: Grid cell decoding hyperparameters

Hyperparameter	Value
Training epochs	200
Learning rate η	0.001
Loss	MSE-Loss
Optimiser	Adam

E. Implementation details

We utilise the `NeuralPlayground`[38] package in order to implement our environment and simulate each of the rodents. `NeuralPlayground` provides a framework for vanilla reinforcement learning (RL) and includes implementations of the successor representation (SR) model for grid cells as introduced by Stachenfeld et al. [8] as well as the gridness score calculations.

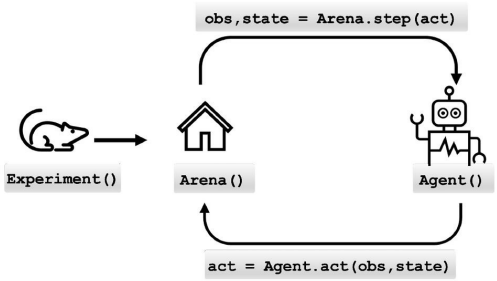

Fig. 11: NeuralPlayground Schematic [38]

Figure 11 illustrates the interaction between the modules of `NeuralPlayground`.

Appendix C
Extended figures and results

A. Alternate representations

Figure 12 illustrates additional grid cell firing patterns to those in Figure 5 with different grid cell periodicities. We additionally illustrate the orientation tuning curves of each and their gridness scores to demonstrate a qualitative view of their regularity. The orientation tuning curves are calculated through rotating the spatial autocorrelation map of the original grid cell pattern for each and computing the correlation of this with the original spatial autocorrelation map. An ideal curve would have peaks at $60°$ and $120°$ and troughs at $30°$ and $90°$. The gridness score is computed using this graph.

B. Gravitational influence

Figures 13, 14 and 15 and 16 illustrate extended versions of Figure 7 across different eigenvectors and added gravity values.

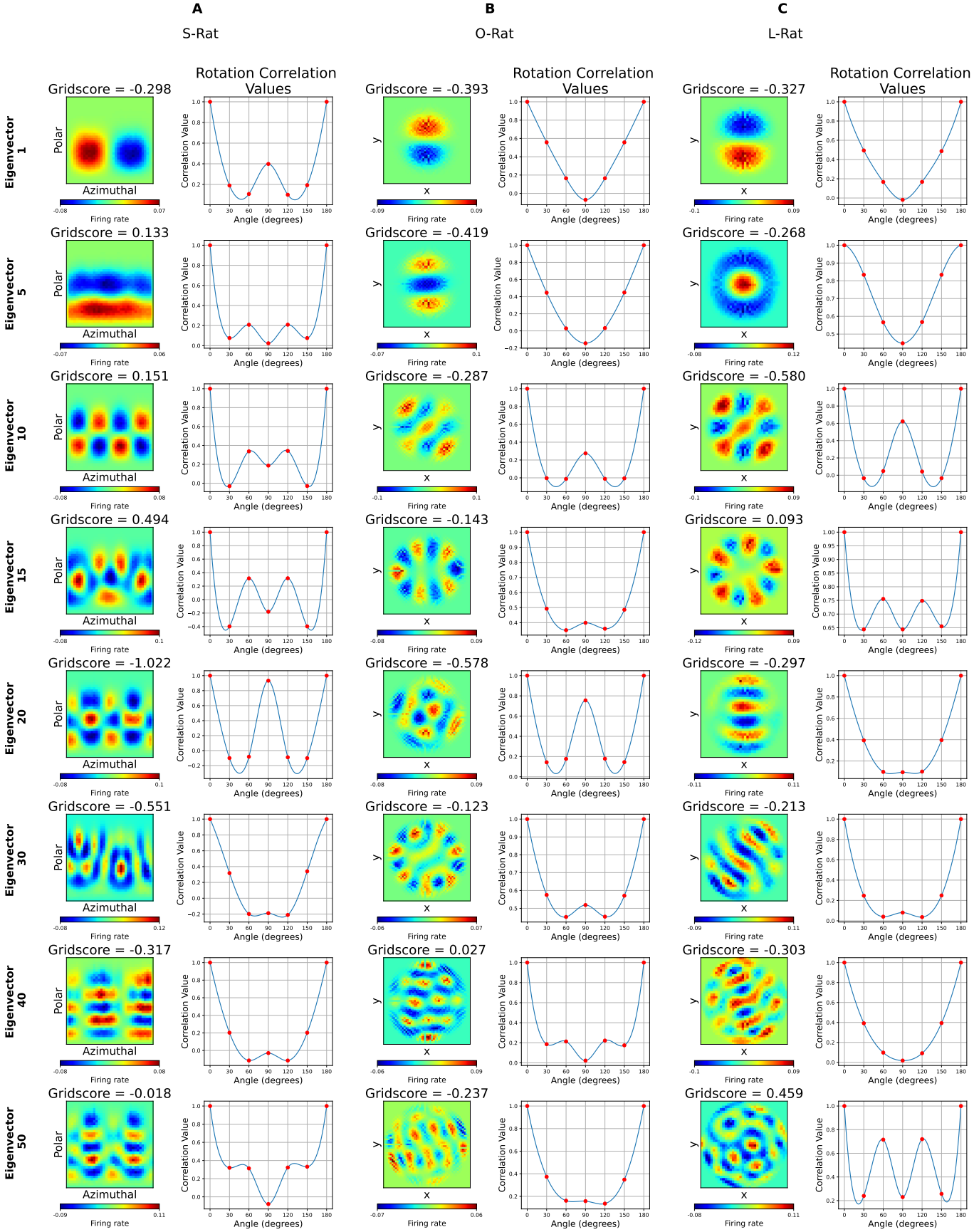

Fig. 12: Extended grid cell predictions from Figure 5. **A**, **B** and **C** depict the grid cell predictions and orientation tuning curves of S-Rat, O-Rat and L-Rat respectively.

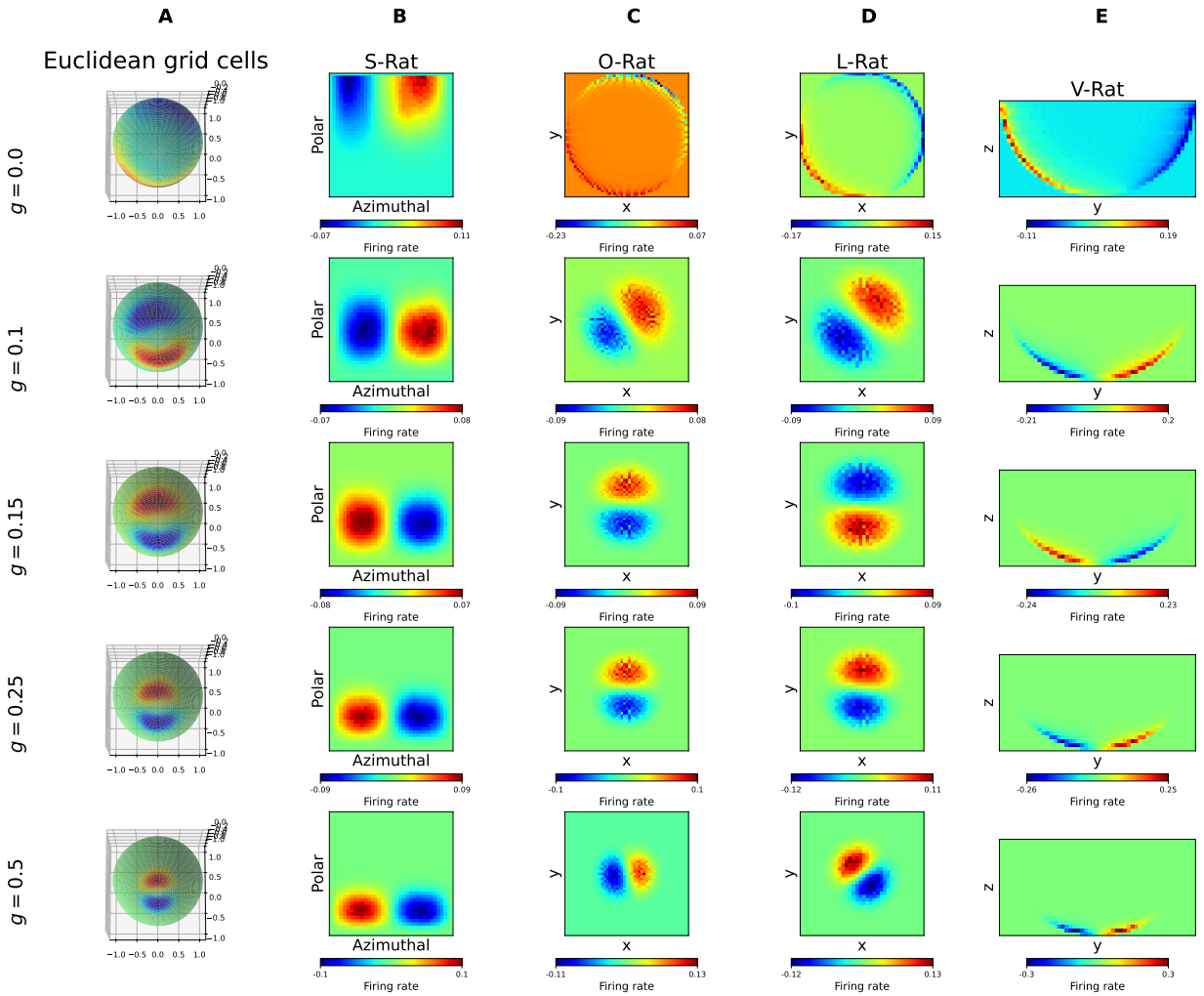

Fig. 13: Extended version of Figure 7 for eigenvector 1.

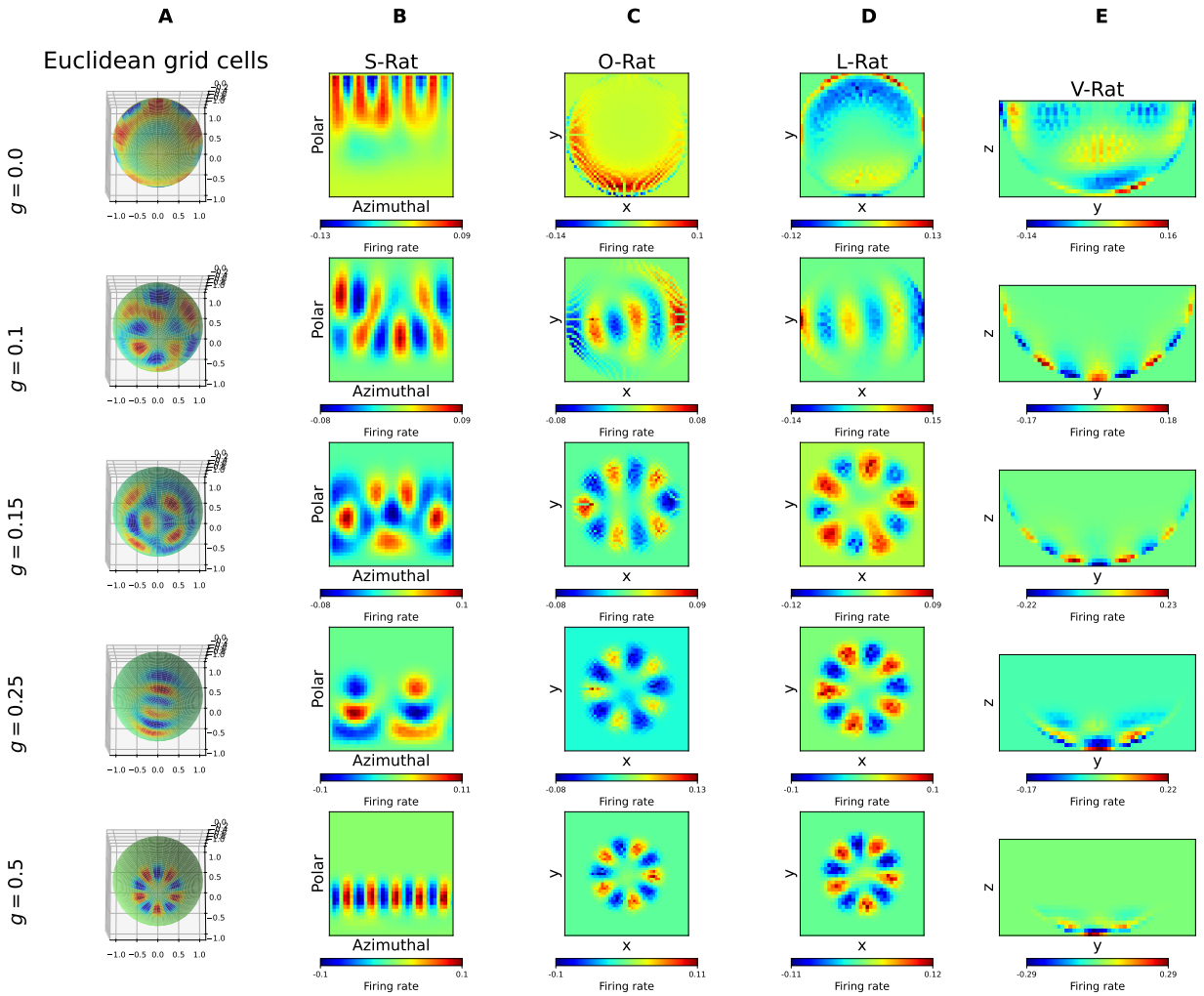

Fig. 14: Extended version of Figure 7 for eigenvector 15.

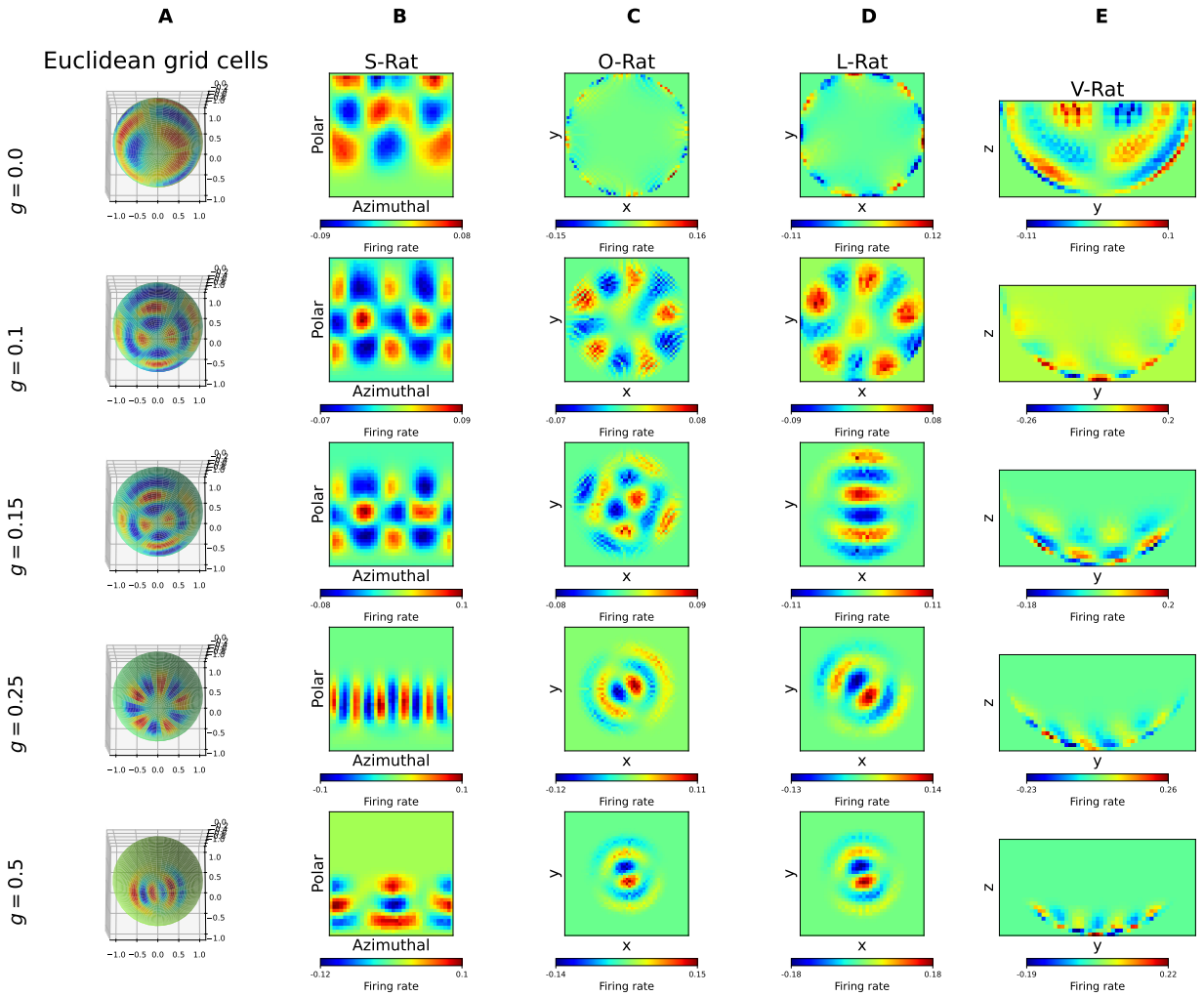

Fig. 15: Extended version of Figure 7 for eigenvector 20.

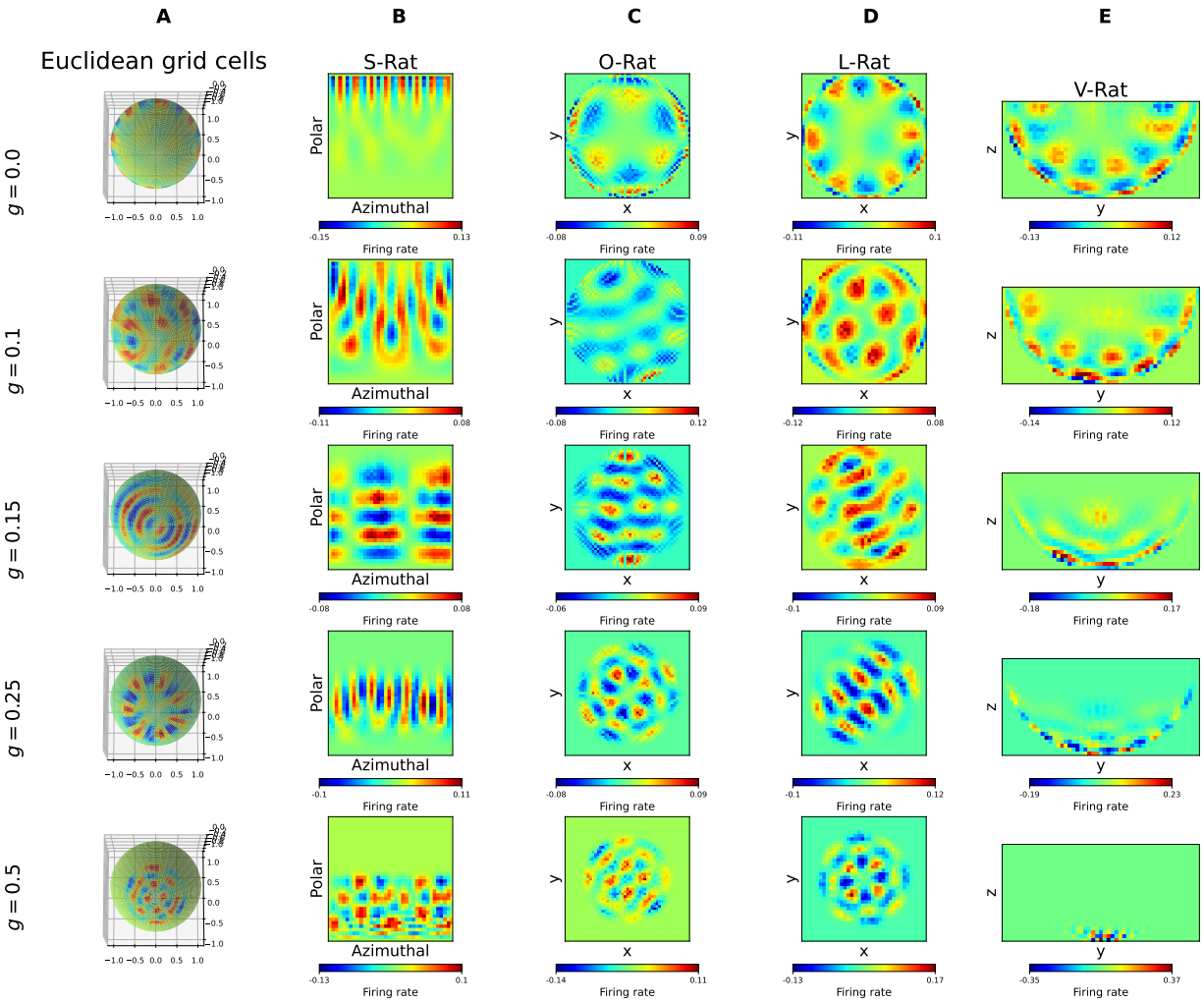

Fig. 16: Extended version of Figure 7 for eigenvector 40.